

6. DATA REPORT: SPINFEX-TEXTURED BASALT XENOLITHS AT PACMANUS, PAPUA NEW GUINEA¹

R.A. Binns^{2, 3}

INTRODUCTION

A number of intensely altered, dark xenoliths with palimpsest quench textures were recorded within altered dacitic host rocks at Site 1189 (Roman Ruins, PACMANUS) during Ocean Drilling Program (ODP) Leg 193. Several of these displayed puzzling marginal fringes, apparently of altered plagioclase with variolitic texture, protruding into adjacent host rocks. Despite their alteration, the xenoliths were interpreted as fragments of rapidly chilled, possibly olivine-bearing basalts incorporated into the dacitic magmas either within the crustal plumbing system or during eruption at the seafloor (figures F15, F16, F17, F42, and F43 in Shipboard Scientific Party, 2002).

An additional example of formerly spinifex-textured xenolith, the first from Site 1188 (Snowcap) and the first from the upper cristobalite-bearing zone of alteration, has been revealed by postcruise studies. Furthermore, a pristine sample of the parent lithology has been found within a dredge haul (MD-138, Binatang-2000 Cruise of *Franklin*; 3°43.60'S, 151°40.35'E, 1688 meters below sea level) from the Satanic Mills hydrothermal field at PACMANUS, near ODP Site 1191.

The purpose of this report is to document these discoveries and thereby to confirm and build on shipboard interpretations. To my knowledge, similar xenoliths have never before been found in modern island arc or backarc volcanic sequences. Spinifex textures are most common in Archean komatiites, some of which are bimodally associated with calc-alkaline felsic volcanic rocks (Barnes et al., 2002).

¹Binns, R.A., 2004. Data report: Spinifex-textured basalt xenoliths at PACMANUS, Papua New Guinea. *In* Barriga, F.J.A.S., Binns, R.A., Miller, D.J., and Herzig, P.M. (Eds.), *Proc. ODP, Sci. Results*, 193, 1–19 [Online]. Available from World Wide Web: <http://www-odp.tamu.edu/publications/193_SR/VOLUME/CHAPTERS/212.PDF>. [Cited YYYY-MM-DD]

²Division of Exploration and Mining, Commonwealth Scientific and Industrial Research Organization (CSIRO), PO Box 136, North Ryde NSW 1670, Australia.

Ray.Binns@csiro.au

³Department of Earth and Marine Sciences, Australian National University, Canberra, ACT 0200 Australia.

METHODS

Samples used for chemical analysis were broken from thin sawn slabs of the respective specimens and carefully hand picked. After ultrasonic cleaning, washing in deionized water to remove sea salt, and drying, the samples were finely ground under acetone in a mechanical agate mortar and pestle. Analyses were performed by X-ray fluorescence (XRF) spectrometry and by inductively coupled plasma–atomic emission spectrometry (ICP-AES) and mass spectrometry (ICP-MS) using the CSIRO methods outlined in Miller et al. (this volume). Loss on drying (LOD; at 105°C) and loss on ignition (LOI; at 1050°C) were measured gravimetrically on separate powder aliquots for three samples. Two handpicked samples of altered dacite were too small for XRF, LOD, or LOI measurements. Table T1 lists preferred data, taking into account precision and sensitivity of the various methods.

Petrological observations were made on polished thin sections. Mineral compositions cited below were obtained with a Cameca Camebax microprobe, fitted with an energy dispersive spectrometer, at the Research School of Earth Sciences, Australian National University (Australia).

RESULTS

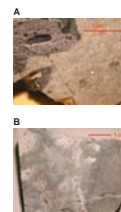
Petrography

The dredged spinifex-textured xenolith from Satanic Mills (CSIRO sample 142421) (Fig. F1A) is enclosed within perfectly glassy, aphyric dacite with numerous vesicles of several size generations. It is disk shaped, ~3 cm thick, and 20 cm in diameter. Its margins are irregular as a consequence of wedging apart by the dacite host. Although there is no fracturing apparent within the xenolith, it was evidently comparatively fluid at the time of incorporation. The quench structure described below persists across the whole xenolith and is not just a marginal feature. Numerous tiny miarolitic cavities and some larger, spherical vesicles are prominent on the hand specimen.

The xenolith fabric (Fig. F2) is dominated by randomly oriented, thin blades of olivine (Fo₇₂₋₈₀) up to 1 cm in length, with hollow cores filled by pyroxene and plagioclase and locally with skeletal margins (Fig. F3). These constitute only ~5% of the volume. Polygonal spaces between the olivine blades are filled by radiating aggregates of sub-parallel pyroxene blades (Figs. F2, F4), between which, in turn, are small, simply twinned laths of plagioclase (An₆₁₋₆₇). Calcic clinopyroxene is predominant, with compositions varying little from Ca₃₉Mg₅₀Fe₁₁ and containing 0.6 wt% TiO₂, 1.8 wt% Al₂O₃, and 0.2 wt% Cr₂O₃. It is accompanied by rarer, more prismatic crystallites of orthopyroxene (Ca₃Mg₇₈Fe₁₉) containing 0.3 wt% TiO₂, 0.9 wt% Al₂O₃, and 0.1 wt% Cr₂O₃. The interstitial plagioclase laths commonly project into miarolitic microcavities (Fig. F4) or extend as circumferential linings on vesicles (Fig. F5) in a manner suggesting that rapid crystallization of the volatile-rich mafic melt has progressed into a supercritical hydrothermal stage. Because the monomineralic plagioclase outgrowths and linings contain no glass or mafic phases, an origin by gas filter-pressing or vapor differentiation (Goff, 1996) is less likely. Tiny crystals of chrome spinel (Al₂₉Cr₅₉Fe³⁺₁₂; Mg/[Mg + Fe²⁺] = 35%) and ilmenite are scattered through the interstices (Figs. F2, F4), and hercynite spinel is a

T1. Compositions of spinifex-textured xenoliths and their hosts, p. 19.

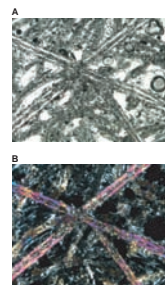
F1. Xenolith of fresh spinifex-textured basalt and xenolith of altered spinifex rock, p. 7.



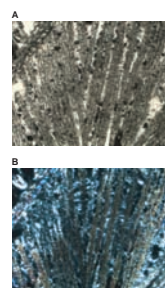
F2. Photomicrograph of spinifex-textured xenolith, p. 8.



F3. Higher-magnification view of spinifex-textured xenolith, p. 9.



F4. Detail of a radiating pyroxene cluster in spinifex rock, p. 10.



rare accompaniment of plagioclase. Subhedral crystals of pyrite (Fig. F2) are a rare and unexplained constituent.

At the xenolith margins, skeletal laths of plagioclase project out into the dacite glass (Fig. F6). Although crystallized from the dacite melt, many of these appear to be epitaxial outgrowths from finer plagioclase between pyroxenes in the adjacent xenolith.

The altered spinifex-textured xenolith revealed by sawing ODP Sample 193-1188A-7R-2 (Piece 1, 17–21 cm; CSIRO 142652) is also discoidal, 1.2 cm across, and at least 4 cm in diameter (Fig. F1B). It is contained within clay-altered, formerly glassy dacite, dissected by numerous cracks adjacent to which the host rock is greenish gray in color for several millimeters. The kernels of larger host remnants between these cracks are very pale green to white in color and possess relic perlitic microfabrics (Fig. F1B). Microscopically, the color changes are associated with Liesegang-like zoning inward from the cracks (Fig. F7). Many but not all of the cracks have been reopened and filled with a succession of cristobalite then cristobalite-anhydrite veins with minor pyrite (Fig. F7), the latter also cutting across the xenolith (Fig. F1B).

The altered xenolith in Sample 193-1188A-7R-2 (Piece 1, 17–21 cm; CSIRO 142652) contains conspicuous dark, randomly oriented blades rich in pyrite (Fig. F1B), not quite so abundant as the olivine blades of the fresh spinifex-textured xenolith (CSIRO dredge sample 142421) but clearly their equivalent. In detail, the fine-grained pyrite replacing the blades is accompanied by clay-chlorite and some fine-grained anhydrite, whereas clay-chlorite in the spaces between blades exhibits a pseudomorphous structure resembling the radiating pyroxene aggregates of the fresh xenolith (Fig. F8). This arises from the distribution of submicroscopic inclusions, probably of rutile, and from slight grain size differences in the clay-chlorite. The matrix is also replaced by abundant anhydrite, ranging from large round grains to dusty particles, and by scarcer pyrite as both larger subhedra and tiny grains (Fig. F8).

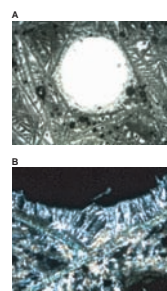
A millimeter-wide rim of paler clay-chlorite with finely disseminated anhydrite at the contact between the altered xenolith and its host (Fig. F9) retains a microfabric highly reminiscent of the epitaxial plagioclase outgrowths seen at this position in the fresh sample. A few more cloudy, needlelike pseudomorphs within this suggest some pyroxene accompanied the plagioclase.

Geochemistry

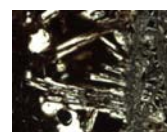
Compositions of the spinifex-textured xenoliths and their hosts are provided in Table T1. The fresh xenolith (142421B) is basaltic with a high MgO content (13.4 wt%), not sufficient to apply the term komatiite (Arndt and Nisbet, 1982) despite the similar quench fabric. In major and trace element compositions, it conforms to but extends the closely constrained fractionation trend displayed by Pual Ridge lavas ranging from basaltic andesite to rhyodacite in composition (Binns et al., 2002), and its glassy dacite host (142421A) also conforms to that trend.

The altered spinifex xenolith (142652D) is significantly depleted in MgO but retains elevated V, Cr, and Ni relative to the fresh rock. High Ca and S reflect the abundance of anhydrite. The two subsamples of brecciated host rock, hand picked free of obvious veins from the white kernel (142652C) and greenish gray rims (142652E), are virtually identical in composition. Their Zr/Ti ratios indicate a dacite parent comparable with the host glass of the fresh sample.

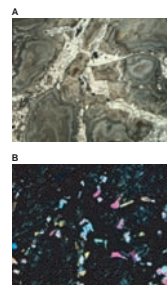
F5. Vesicle lined by simply twinned plagioclase laths, p. 11.



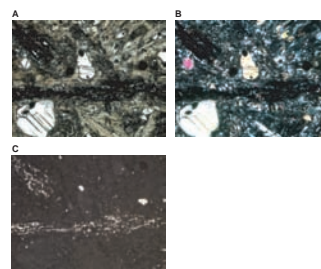
F6. Contact between spinifex-textured xenolith and dacite host, p. 12.



F7. Network of cristobalite-anhydrite-(pyrite) veins, p. 13.



F8. Fine-grained intergrowths of pyrite, chloritic clay, and minor anhydrite, p. 14.



F9. Contact between altered spinifex-textured xenolith and altered dacite host, p. 15.

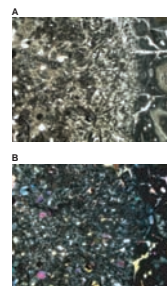


Figure F10 plots gains and losses of particular elements during alteration relative to the appropriate portion of the fresh rock. This ignores the effects of volume changes and hydration but clearly shows extreme enrichment in S and Te during alteration of all three altered samples and substantial depletions in alkali elements, Mn, and Mg in most.

Figure F11 displays the differing behavior of the rare earth elements (REE). The flat chondrite-normalized REE pattern of the fresh spinifex xenolith compares closely with other basaltic rocks from the eastern Manus Basin, while the dacite glass shows the higher abundances and the light REE enrichment characteristic of the more fractionated lavas. Relative to its fresh equivalent, the altered spinifex-textured xenolith has similar light and mid-REE abundances but mildly depleted heavy REE. The two host rock samples have very different REE characteristics. The white kernel (142652C) shows pronounced overall reduction in abundance, with La and Ce being slightly more depleted relative to the mid-REE and a slightly greater progressive depletion in the heavier REE. The green rim material (142652E), despite its otherwise geochemical similarity with the white kernel, shows a greater level of overall depletion in REE and pronounced relative loss of the light REE from La to Nd.

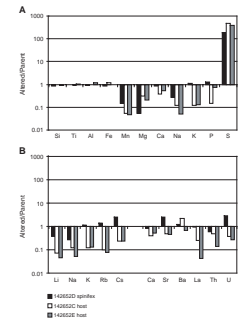
DISCUSSION

The discovery of a fresh spinifex-textured basalt xenolith in glassy dacite, dredged from the seafloor at Satanic Mills, confirms the interpretations assigned by Shipboard Scientific Party (2002), based on textures, to the altered equivalents encountered in Holes 1189A and 1189B at Roman Ruins. The additional altered xenolith now found in Hole 1188A, described here, extends the lateral range of such occurrences to the Snowcap site, and we can now say with confidence that spinifex-textured xenoliths occur throughout the vertical sequence of lavas by which Pual Ridge is constructed.

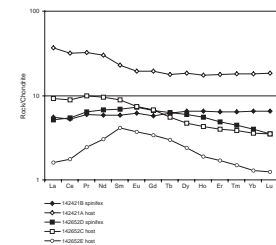
No outcropping spinifex-textured lavas have been recorded despite intense dredging and bottom photography along the crest of Pual Ridge or anywhere else in the eastern Manus Basin. Hence, it is more likely that the xenoliths derive from deep within the igneous system. Were they accidentally broken from the quenched margin of a subjacent mafic intrusion, one might expect fragments from more slowly cooled interiors to occur as well.

The possibility is noted above that the fresh spinifex-textured xenolith was relatively fluid, perhaps incompletely crystallized, when incorporated within the dacitic melt. A long-standing puzzle regarding the felsic lavas at Pual Ridge is their apparently high eruption temperatures, at or above their liquidus, as indicated by an essentially aphyric nature and their fluidity as evidenced by lava structures more commonly associated with mafic melts (Waters et al., 1996; Waters and Binns, 1998). The latter include lobate and pillowlike structures and the presence of drained collapse pits. Reheating within a fractionating magma chamber by the introduction of fresh batches of parental basalt magma is the possible explanation. The major and trace element geochemistry of the fresh spinifex-textured xenolith conforms to the requirements of a potential parent magma for the Pual Ridge fractionation sequence (basaltic andesite through andesite and dacite to rhyodacite). Conceivably, the xenolith and its drilled equivalents represent lobes detached from a fresh magma batch and incorporated into a fractionated melt in the

F10. Diagrams illustrating mass changes during alteration, p. 16.



F11. Chondrite-normalized REE profiles, p. 18.



chamber, becoming itself quenched while causing overheating of the latter.

Although it contains no hydrous minerals, vesicularity of the fresh spinifex-textured xenolith indicates that the melt from which it crystallized rapidly was distinctly hydrous. An interesting possibility deserving further study, suggested by plagioclase rims on vesicles and miarolitic cavities, is that initial igneous crystallization of the mafic silicate melt caused increase in the proportion of water to such an extent that final crystallization was under supercritical hydrothermal conditions, in a manner akin to the formation of pegmatites in granite bodies.

ACKNOWLEDGMENTS

Lesley Dotter and Mike Hart of CSIRO performed the ICP and XRF analyses, respectively. This research used samples provided by the Ocean Drilling Program (ODP). ODP is sponsored by the U.S. National Science Foundation (NSF) and participating countries under management of Joint Oceanographic Institutions (JOI), Inc. Funding was provided by CSIRO and the P2+ consortium of Australian mineral companies.

REFERENCES

- Arndt, N.T., and Nisbet, E.G., 1982. *Komatiites*: London (George Allen and Unwin).
- Barnes, S.J., Hill, R.E.T., Thordarson, T., Dowling, S.E., and Mattox, T.N., 2002. Bimodal komatiite-dacite volcanism in the Black Swan area, Norseman-Wiluna greenstone belt, Australia. *Geochim. Cosmochim. Acta*, 66(15A):53.
- Binns, R.A., McConachy, T.F., Parr, J.M., and Yeats, C.J., 2002. The PACMANUS Memoir (P2+). *CSIRO Exploration and Mining Report 1032C* [CD-ROM]. Available from: CSIRO Exploration and Mining, North Ryde NSW 1670, Australia.
- Goff, F., 1996. Vesicle cylinders in vapor-differentiated basalt flows. *J. Volcanol. Geotherm. Res.*, 97:167–185.
- Shipboard Scientific Party, 2002. Site 1189. In Binns, R.A., Barriga, F.J.A.S., Miller, D.J., et al., *Proc. ODP, Init. Repts.*, 193 [CD-ROM]. Available from: Ocean Drilling Program, Texas A&M University, College Station TX 77845-9547, USA.
- Waters, J.C., and Binns, R.A., 1998. Contrasting styles of felsic submarine volcanism, eastern Manus Basin, Papua New Guinea. *Geol. Soc. Aust., Abstr. Ser.*, 49:459.
- Waters, J.C., Binns, R.A., and Naka, J., 1996. Morphology of submarine felsic volcanic rocks on Pual Ridge, eastern Manus Basin, Papua New Guinea. *Eos, Trans. Am. Geophys. Union*, 77:W120.

Figure F1. A. Xenolith of spinifex-textured basalt within vesicular dacite glass, dredged at Satanic Mills (CSIRO sample 142421, dredge MD-138). The xenolith also contains small vesicles and miarolitic cavities between olivine blades. It appears wedged apart without fracturing by dacite glass at upper right and lower left. B. Altered xenolith of spinifex rock in altered and veined dacite (Sample 193-1188A-7R-2 [Piece 1, 17–21 cm]; CSIRO 142652). Former olivine blades in the xenolith are replaced by pyrite. Both the xenolith and its host are cut by a network of anhydrite-cristobalite veins. A later vein of coarse anhydrite occurs along the upper edge of the specimen.

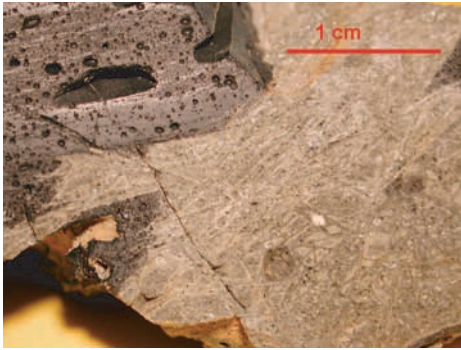
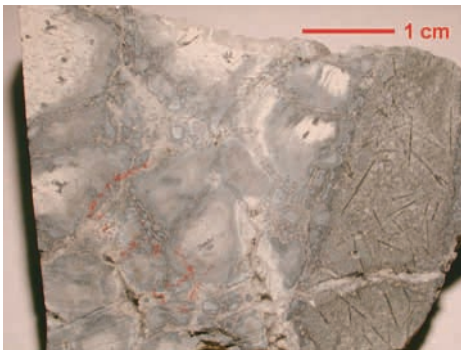
A**B**

Figure F2. Photomicrograph of spinifex-textured xenolith in CSIRO sample 142421. Larger, randomly oriented blades are olivine. The triangular spaces between olivines are occupied by radiating plates of pyroxene, with interstitial plagioclase laths that in places protrude into tiny miarolitic cavities. Large black grain is pyrite; others are ilmenite and chrome spinel. Width of view = 5.0 mm; ordinary transmitted light.

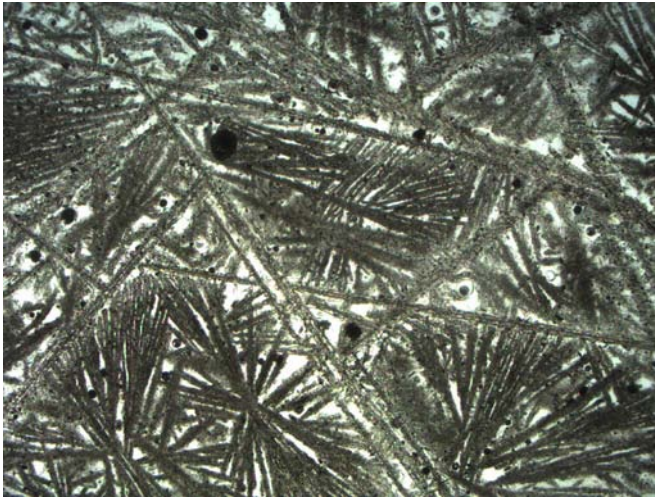


Figure F3. Higher-magnification view of spinifex-textured xenolith in CSIRO sample 142421. Birefringent olivine blades are skeletal, with fine pyroxene-plagioclase cores. Plagioclase laths (twinned with gray birefringence colors in lower frame) between pyroxene platelets commonly project into miarolitic cavities, some of which are occupied by bubbles in the epoxy mounting medium. Opaque grains are ilmenite. Width of view = 1.3 mm; (A) ordinary light, (B) crossed polarizers.

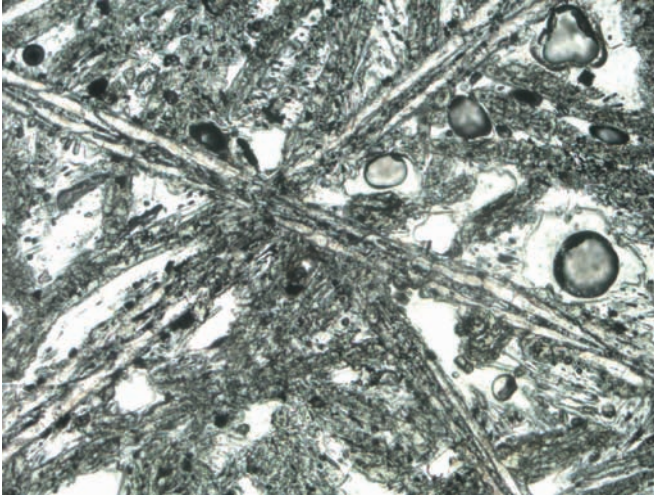
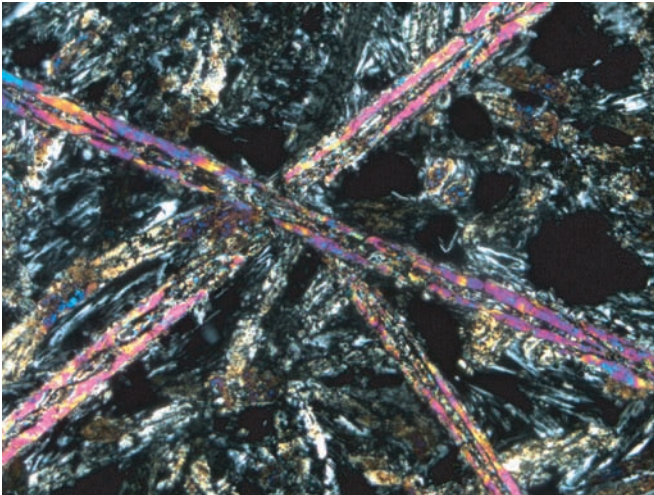
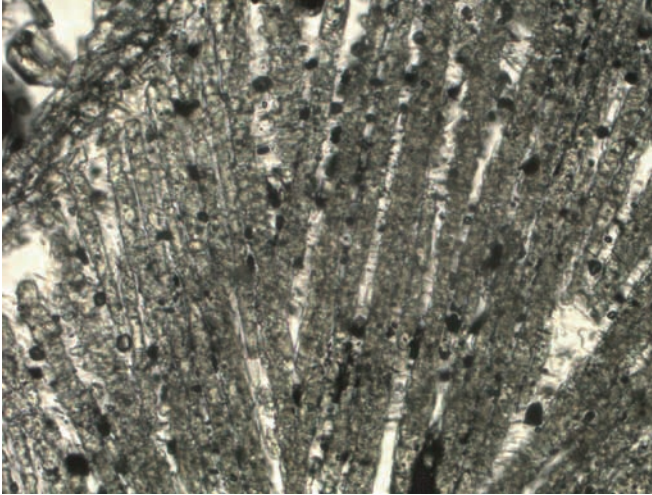
A**B**

Figure F4. Detail of a radiating pyroxene cluster in spinifex rock (CSIRO sample 142421), with tiny interstitial laths of plagioclase. A small miarolitic cavity lined with plagioclase occurs at the lower right. Width of view = 0.64 mm; (A) ordinary light, (B) crossed polarizers.

A



B

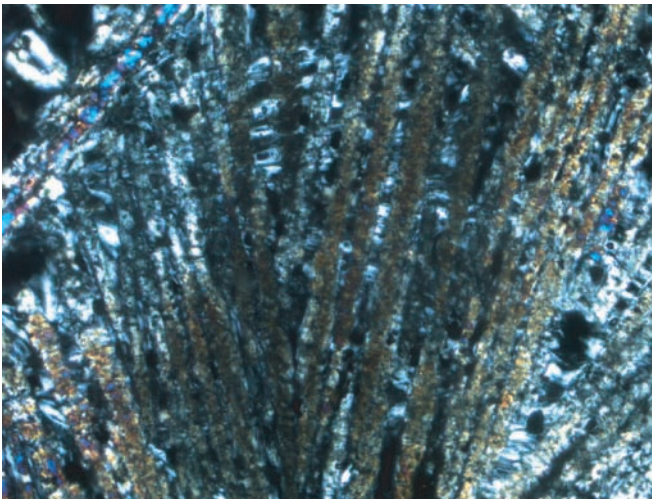
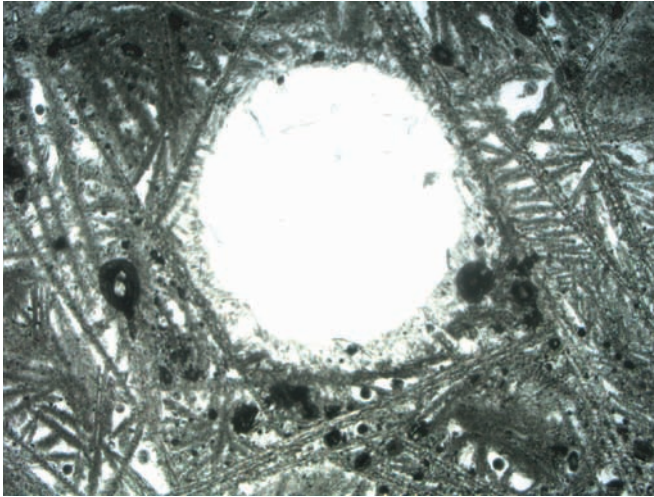


Figure F5. Vesicle lined by simply twinned plagioclase laths, set between pyroxene platelets in spinifex rock (CSIRO sample 142421). Widths of view = (A) 5.0 mm, ordinary light; (B) 1.3 mm, crossed polarizers.

A



B

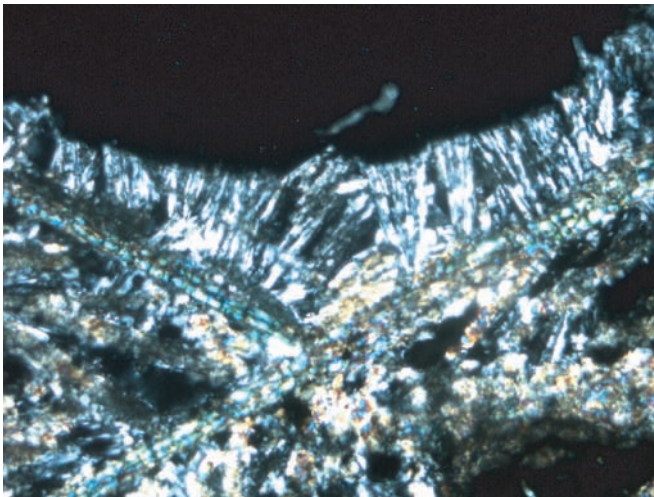


Figure F6. Contact between spinifex-textured xenolith (right) and vesicular, brown glassy dacite host (left) in CSIRO sample 142421. Skeletal laths of plagioclase projecting into the dacite glass are epitaxial outgrowths from those in the xenolith. Width of view = 0.64 mm; ordinary light.

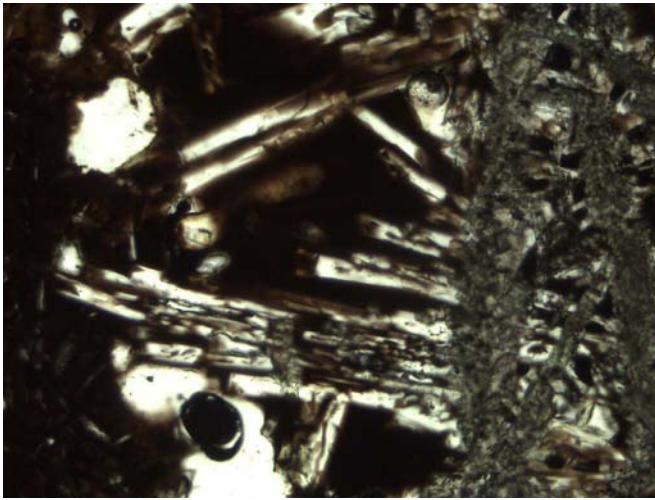


Figure F7. Network of cristobalite-anhydrite-(pyrite) veins in altered dacite host portion of Sample 193-1188A-7R-2 [Piece 1, 17–21 cm]; CSIRO 142652). Layers of tiny pyrite grains define the Liesegang-like alteration of a former, possibly perlitic glass. Low birefringence clay replacing the glass has a plumose structure extending across these layers. Width of view = 5.0 mm; (A) ordinary light, (B) crossed polarizers.

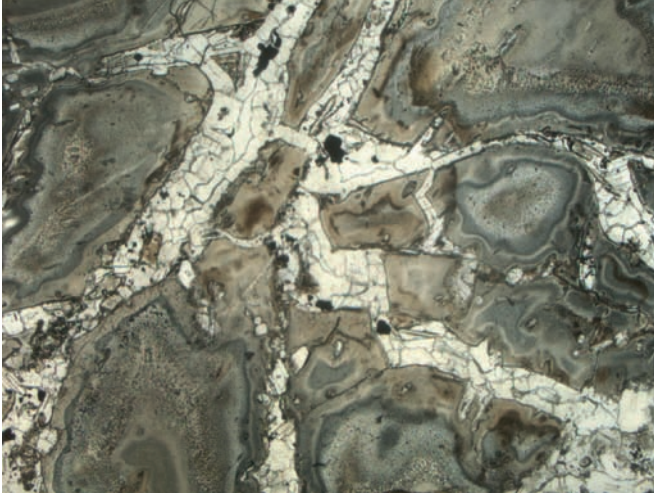
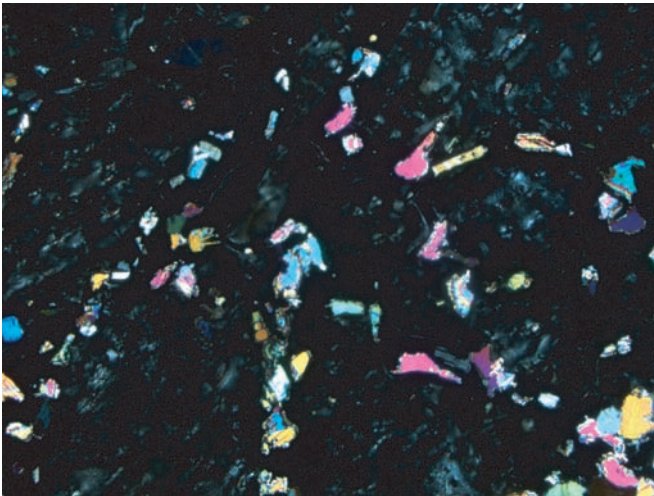
A**B**

Figure F8. Former olivine blades, replaced by fine grained intergrowths of pyrite, chloritic clay, and minor anhydrite, in the spinifex-textured xenolith within altered dacite Sample 193-1188A-7R-2 (Piece 1, 17–21 cm; CSIRO 142652). Pseudomorphs of former radiating pyroxene platelets between the olivine blades, replaced by clay, are evident in the ordinary light view (A). Large euhedra of pyrite and anhedral, birefringent anhydrite, plus tiny equivalents, together with clay, have replaced the matrix. Width of view = 1.3 mm; (A) ordinary transmitted light, (B) transmitted light with crossed polarizers, (C) reflected light.

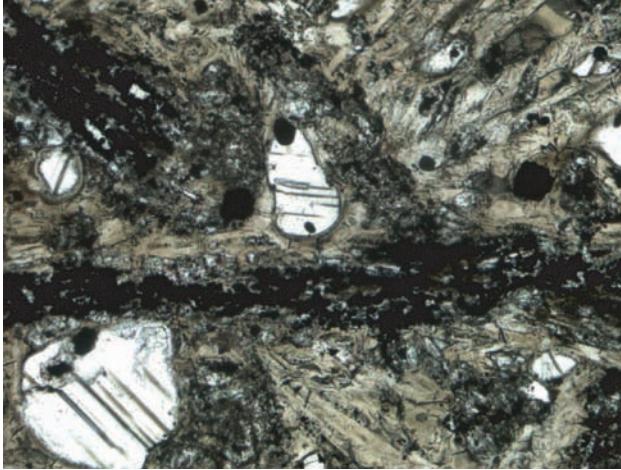
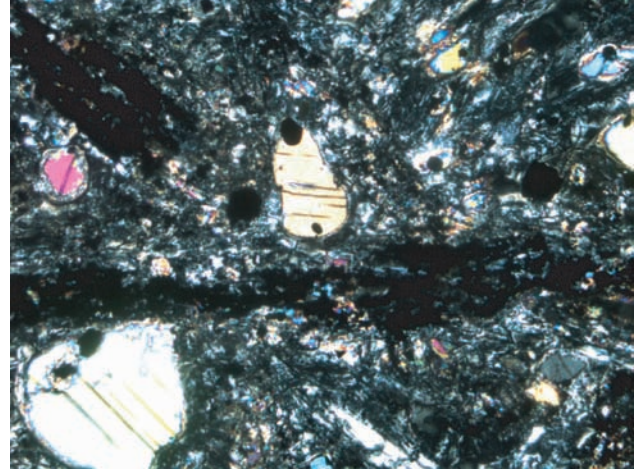
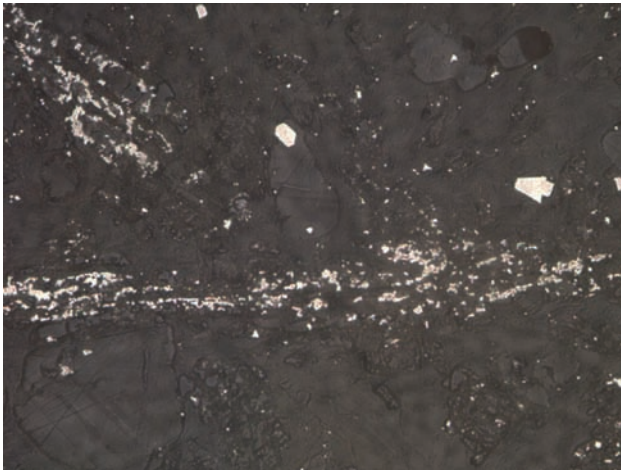
A**B****C**

Figure F9. Contact between altered spinifex-textured xenolith (left) and altered dacite host (right) in Sample 193-1188A-7R-2 (Piece 1, 17–21 cm; CSIRO 142652). Despite complete alteration to clay and permeation by anhydrite, the microfabric is preserved of a former marginal outgrowth of plagioclase laths from xenolith into host (compare Fig. F6, p. 12). Width of view = 5 mm; (A) ordinary light, (B) crossed polarizers.

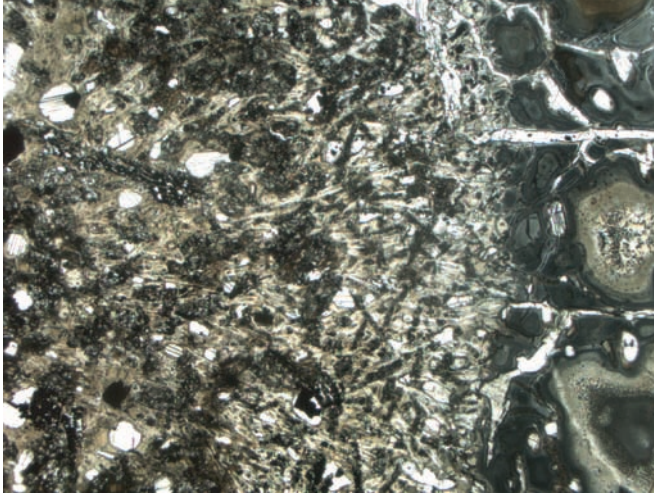
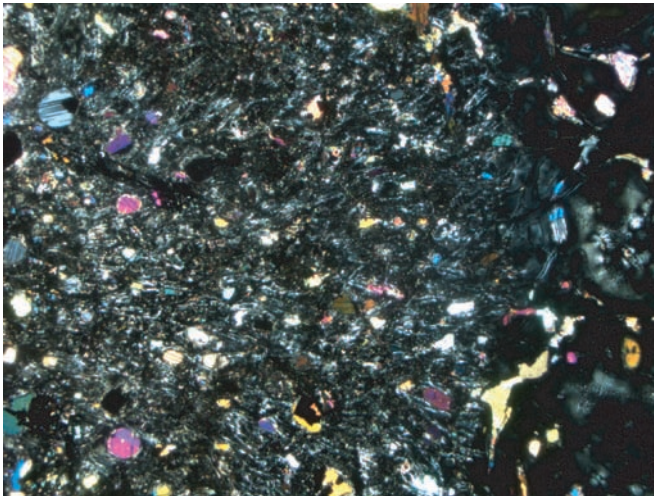
A**B**

Figure F10. Diagrams illustrating mass changes during alteration of spinifex xenolith and its host in Sample 193-1188A-7R-2 (Piece 1, 17–21 cm; CSIRO 142652). (A) major elements, (B) alkalis and alkali earths. (Continued on next page.)

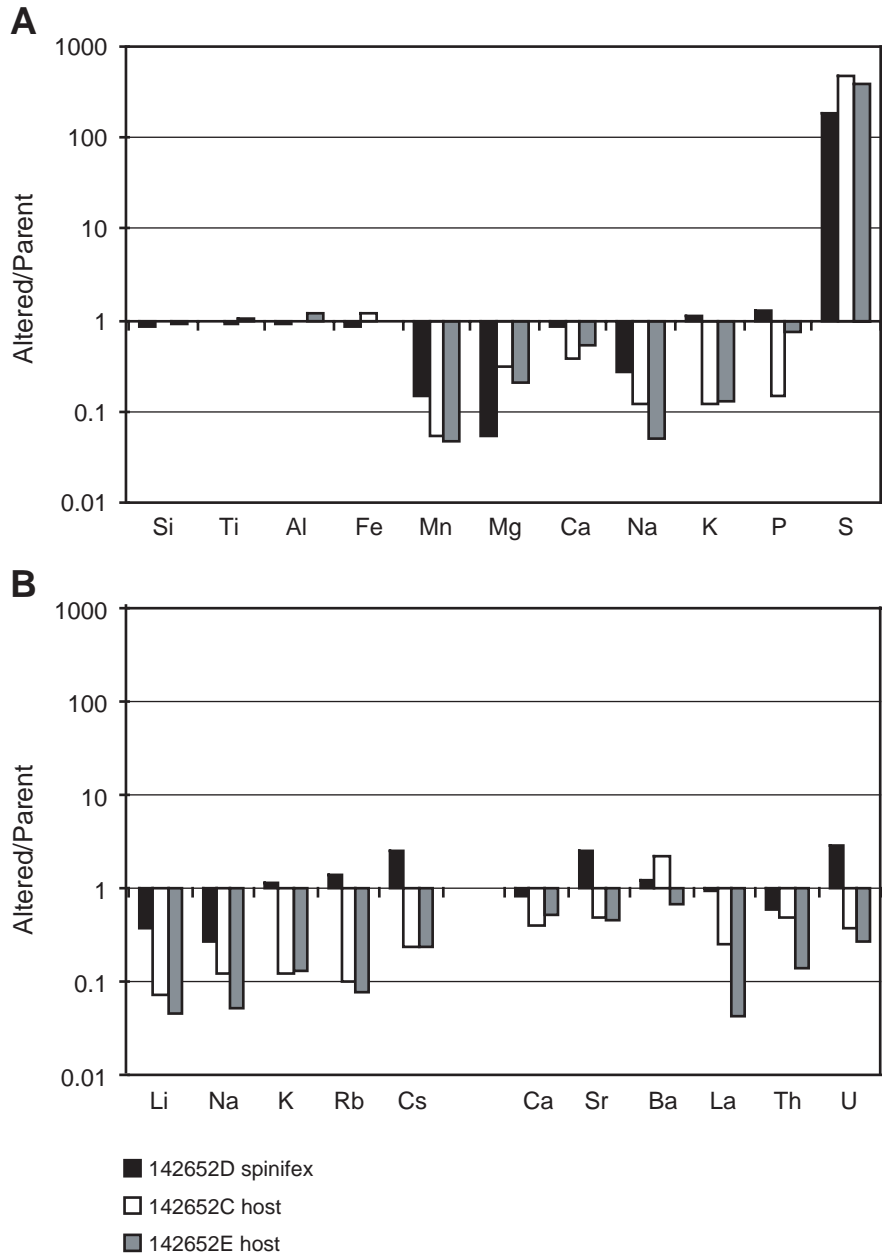


Figure F10 (continued). (C) metals, (D) chalcophile metals and nonmetals.

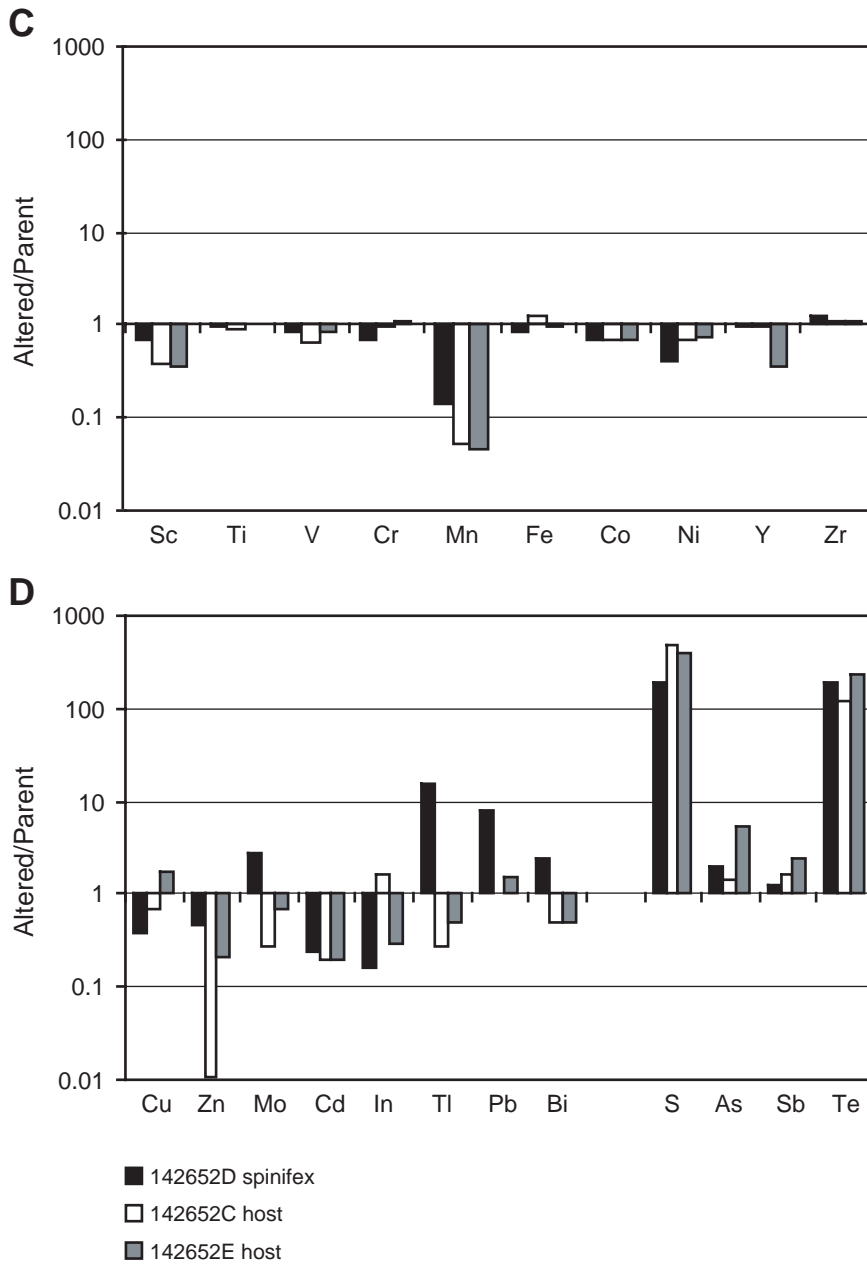


Figure F11. Chondrite-normalized REE profiles for fresh and altered spinifex rocks (solid symbols) and their hosts (open symbols).

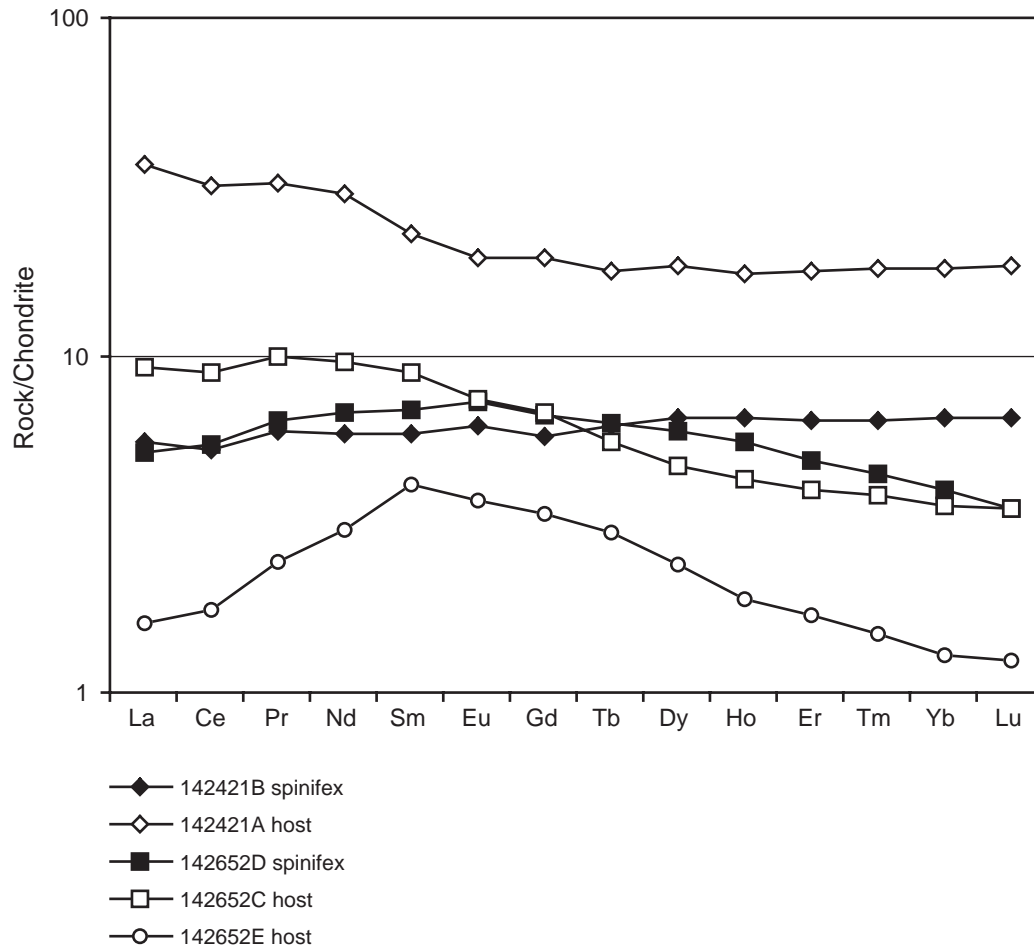


Table T1. Compositions of spinifex-textured xenoliths and their hosts.

Major Element/Oxide:	SiO ₂	TiO ₂	Al ₂ O ₃	FeO (total)	MnO	MgO	CaO	Na ₂ O	K ₂ O	P ₂ O ₅	S (total)	LOD	LOI	Total		
Units:	wt%	wt%	wt%	wt%	wt%	wt%	wt%	wt%	wt%	wt%	wt%	wt%	wt%	wt%		
CSIRO number	Method:	XRF	XRF	XRF	XRF	XRF	XRF	XRF	XRF	XRF	ICP-AES					
Spinifex xenoliths																
142421B*		50.80	0.42	12.76	8.12	0.18	13.43	10.59	2.08	0.23	0.056	0.06	0.24	0.12	99.08	
142652D†		42.75	0.40	11.28	6.72	0.026	0.71	8.90	0.56	0.25	0.070	11.53	2.20	10.87	96.26	
Host rocks																
142421A*		66.39	0.72	14.28	4.93	0.15	1.11	3.42	5.01	1.65	0.175	0.01	0.25	1.15	99.24	
142652C†		64.31‡	0.64‡	14.09‡	6.00‡	0.008‡	0.33‡	1.32‡	0.62‡	0.20‡	0.025‡	6.19	NA	NA	93.75	
142652E†		62.22‡	0.72‡	16.46‡	4.79‡	0.007‡	0.23‡	1.80‡	0.26‡	0.22‡	0.133‡	5.06	NA	NA	91.90	
Trace element:	Li	Be	Cl	Sc	V	Cr	Co	Ni	Cu	Zn	Ga	Ge	As	Rb	Sr	
Units:	ppm	ppm	ppm	ppm	ppm	ppm	ppm	ppm	ppm	ppm	ppm	ppm	ppm	ppm	ppm	
CSIRO number	Method:	ICP-AES	ICP-AES	XRF	ICP-MS	ICP-MS	ICP-MS	ICP-MS	ICP-MS	ICP-AES	ICP-AES	ICP-MS	ICP-MS	ICP-MS	ICP-MS	
Spinifex xenoliths																
142421B		3.1	0.31	6690	36	203‡	800	57	328‡	107	91	12	2.5	8.7	3.0	121
142652D		1.14	0.63	2818	25	169‡	552	40	133‡	40	44	16	1.4	18	4.4	298
Host rocks																
142421A		12.7	1.11	4500	16	44	17	8.3	9.1	27	91	21	3.1	4.8	32	290
142652C		0.92	0.72	NA	6.2	29	16	5.6	6.5	18	1.0	19	2.2	6.6	3.2	139
142652E		0.58	0.93	NA	5.8	37	18	5.6	6.8	46	20	19	1.7	25	2.5	131
Trace element:	Y	Zr	Mo	Cd	In	Sb	Te	Cs	Ba	La	Ce	Pr	Nd	Sm	Eu	
Units:	ppm	ppm	ppm	ppb	ppb	ppb	ppb	ppb	ppm	ppm	ppm	ppm	ppm	ppm	ppm	
CSIRO number	Method:	ICP-AES	XRF	ICP-MS	ICP-MS	ICP-MS	ICP-MS	ICP-MS	ICP-AES	ICP-MS	ICP-MS	ICP-MS	ICP-MS	ICP-MS	ICP-MS	
Spinifex xenoliths																
142421B		12	23	1.1	315	131	701	20	90	115	2.03	4.98	0.81	4.19	1.35	0.537
142652D		12	30	3.0	76	22	868	3779	231	136	1.90	5.19	0.88	4.81	1.60	0.637
Host rocks																
142421A		30	107	2.3	383	87	309	10	794	303	13.50	30.27	4.46	21.31	5.29	1.702
142652C		29	120‡	0.63	73	146	495	1253	186	666	3.38	8.49	1.36	6.84	2.04	0.650
142652E		11	114‡	1.6	76	25	738	2432	182	206	0.59	1.69	0.33	2.17	0.95	0.326
Trace element:	Gd	Tb	Dy	Ho	Er	Tm	Yb	Lu	Tl	Pb	Bi	Th	U			
Units:	ppm	ppm	ppm	ppm	ppm	ppm	ppm	ppm	ppb	ppm	ppb	ppb	ppb			
CSIRO number	Method:	ICP-MS	ICP-MS	ICP-MS	ICP-MS	ICP-MS	ICP-MS	ICP-MS	ICP-MS	ICP-MS	ICP-MS	ICP-MS	ICP-MS			
Spinifex xenoliths																
142421B		1.75	0.360	2.51	0.558	1.58	0.227	1.61	0.249	29	2.7	43	197	126		
142652D		2.04	0.366	2.27	0.470	1.22	0.160	0.98	0.135	453	21	104	113	354		
Host rocks																
142421A		5.99	1.037	6.96	1.491	4.45	0.641	4.44	0.703	251	7.2	98	1527	832		
142652C		2.08	0.321	1.78	0.367	0.99	0.136	0.89	0.133	71	7.3	48	722	309		
142652E		1.04	0.172	0.92	0.160	0.43	0.053	0.32	0.048	128	11	50	209	218		

Notes: * = dredge MD-138; 3°43.60'S 151°40.35'E. † = ODP Sample 193-1188A-7R-2 (Piece 1, 17–21 cm). Sample 142421A = dacite glass, Sample 142652C = handpicked white kernel of fragment in brecciated host rock. Sample 142652E = handpicked pale green rims from fragments in brecciated host rock. ‡ = ICP-AES data, cited where analyses by the primary method were over range or unavailable. LOD = loss on drying at 105°C (samples pre-dried at ~40°C). LOI = loss on ignition at 1050°C. NA = not analyzed.